RESEARCH ARTICLE | SEPTEMBER 08 2025

Optical properties of intrinsic vacancy and interstitial defects in AlN ⊕

Lei Zhu ⓘ ; Xingfan Zhang ⓘ ; You Lu ⓘ ; Thomas W. Keal ⓘ ; John Buckeridge ⓘ ;
C. Richard A. Catlow ✉ ⓘ ; Alexey A. Sokol ⓘ

Check for updates

View Online   Export Citation

Articles You May Be Interested In

Hole localization in [AlO 4] defects in silica materials

J. Chem. Phys. (April 2005)

Optical excitations of defects in realistic nanoscale silica clusters: Comparing the performance of density functional theory using hybrid functionals with correlated wavefunction methods

J. Chem. Phys. (July 2008)

Prediction of multiband luminescence due to the gallium vacancy–oxygen defect complex in GaN

Appl. Phys. Lett. (June 2018)

AIP Publishing

Optical properties of intrinsic vacancy and interstitial defects in AlN (EP)

Lei Zhu,[1,2] (ID) Xingfan Zhang,[1] (ID) You Lu,[3] (ID) Thomas W. Keal,[3] (ID) John Buckeridge,[4,5] (ID)
C. Richard A. Catlow,[1,6,a)] (ID) and Alexey A. Sokol[1,b)] (ID)

AFFILIATIONS

[1] Department of Chemistry, University College London, 20 Gordon St., London WC1 HOAJ, United Kingdom

[2] Department of Materials, University of Oxford, Park Road, Oxford OX1 3PH, United Kingdom

[3] STFC Scientific Computing, Daresbury Laboratory, Keckwick Lane, Daresbury WA4 4AD, United Kingdom

[4] School of Engineering and Design, London South Bank University, 103 Borough Road, London SE1 0AA, United Kingdom

[5] Energy, Materials and Environment Research Centre, London South Bank University, 103 Borough Road, London SE1 0AA, United Kingdom

[6] School of Chemistry, Cardiff University, Main Building, Park Place, Cardiff CF10 3AT, United Kingdom

[a)]**Author to whom correspondence should be addressed:** c.r.a.catlow@ucl.ac.uk
[b)]a.sokol@ucl.ac.uk

ABSTRACT

Aluminum nitride (AlN), a wide-band-gap semiconductor, is a key material for ultraviolet optoelectronics and emerging quantum technologies. However, its performance is significantly affected by intrinsic point defects that introduce deep and shallow levels within the bandgap. Here, we combine a hybrid quantum mechanical/molecular mechanical embedded cluster approach with direct comparison to photoluminescence and cathodoluminescence measurements to investigate the optical transition properties of the four most stable intrinsic point defects in AlN: aluminum vacancies, nitrogen vacancies, aluminum interstitials, and nitrogen interstitials. Calculated configuration-coordinate diagrams across all relevant charge states enable the assignment of experimentally observed optical bands to specific defect-related transitions. Our results highlight N vacancies as the dominant contributors to optical signals under most growth conditions. Although we find that Al vacancies are frequently associated with blue-to-UV optical transitions, their actual contribution remains uncertain due to the dependence of their formation on donor-rich environments. N split-interstitials also play a significant role depending on concentrations and growth conditions. This theoretical analysis, grounded firmly in suitable experimental compaisons, advances the understanding of defect-related optical properties in AlN and offers guidance for the design of optoelectronic and quantum devices.

I. INTRODUCTION

Aluminum nitride (AlN) is an advanced semiconductor material widely recognized for its applications in optoelectronic devices and quantum information systems, particularly in environments demanding high-power operation and robustness at high temperatures.[1] Its wide 6.2 eV bandgap makes the material an excellent candidate for ultra-violet-spectrum (UV) light emitting diodes (LEDs)[2–4] and laser diodes.[5] High concentrations of various point defects in AlN, which can create deep and shallow recombination states within the bandgap, hinder optimal optical performance and operational stability in these UV-LED devices.[4,6] Notably, with the growing prominence of quantum technology, these deep defect centers in wide-band-gap semiconductors characterized by strongly localized spin states are increasingly considered to be promising hosts for quantum bits (qubits), enabling applications such as single-photon emitters.[7,8] The remarkable versatility of AlN underscores the need for further investigation into its defect properties.

The challenge of identifying the origin of shallow and deep states lies in the difficulty of determining whether they arise from

a single defect species or a collective of multiple species. Optical characterization techniques, such as photoluminescence (PL) and cathodoluminescence (CL), serve as valuable tools for probing the transition energies between energy bands and defect states. These techniques also aid in assigning defect species to the states, mostly by matching optical signals with defect charge transition levels calculated using density functional theory (DFT) methods. This approach assumes that any optical transition between the valence band (VB)/conduction band (CB) and any defect states corresponds to a change in the defect's charge state, provided that the charge carriers are strongly localized at the defect centers. While this approach provides a good approximation of transitions between two structurally relaxed defect states, it does not fully capture the origin of these transitions, particularly when phonon-coupled transitions are involved, as optical transitions occur much faster than structural relaxations. As summarized in Table I, a broad spectrum of optical signals has so far been attributed to intrinsic aluminum and nitrogen vacancies.

DFT-based methods for defect chemistry have been extensively developed over the years, evolving into a powerful tool for calculating the structural and electronic properties of native defects and impurities in semiconductor materials. These techniques have been applied to defect analysis in AlN,[18,22–40] mainly using plane-wave based approaches, in which an infinite periodic system is represented by a single unit cell image and simulated under specific periodic boundary conditions. While these approaches offer many advantages for modeling periodic crystalline material systems, limitations such as finite-size effects[41] and scaling challenges restrict their suitability for higher-level DFT analyses of point defects in very large systems. Furthermore, for charged defects, these methods often struggle to describe accurately long-range interactions and polarization effects, leading to inaccuracies in describing the ionization process. Such errors can only be approximately corrected *a posteriori*.[42] Early attempts to address these issues included the use of an embedded quantum cluster method, enabling the modeling of point defects in systems approaching the dilute limit.[43,44] As a result, the ionization process of the charge-changing defect

species benefits from an unambiguous reference, which is more physically reasonable. However, those studies only examined two types of point defect species in zinc-blende AlN using a small five-atom AlN cluster for the DFT region. In the present work, we employ a more advanced hybrid quantum mechanical molecular mechanical (QM/MM) method[45] to investigate the four most stable intrinsic point defect types, using a much larger quantum mechanical cluster and a more robust interatomic potential model (more details in Sec. II), providing an accurate treatment for polarisation of the host material by defects. As a result, our QM/MM system provides more accurate formation energies for charged point defects and the energy levels of all defect states within the bandgap.

In our previous work using the QM/MM method, intrinsic point defects in AlN were investigated using a defect transition diagram,[46] which is a commonly used diagram for comparing the thermodynamic stability of different point defect types and analyzing the charge transitions between various charge states of defect species. Our simulations suggest that the aluminum vacancy (in the Kröger–Vink notation: V_{Al}), nitrogen vacancy (V_N), aluminum interstitial (Al_i), and nitrogen interstitial (N_i) are the four most stable intrinsic point defects in AlN.[46] Other reported intrinsic defects, such as antisite defects, are excluded from this study, as they are predicted to have significantly lower concentrations and minimal impact on the optical signals of the material. In this work, we study the optical transition properties of these four intrinsic defect types by systematically applying configuration-coordinate diagrams to all the charge states. This allows us to use the predicted Fermi level to screen all possible defect origins of the optical transitions under different crystal growth conditions and to expand the analysis to a wider range of defect species, such as interstitial defects. We identify N vacancies as the primary contributor to optical signals due to their high stability and prevalence under most crystal growth conditions. Al vacancy and N split-interstitial defects can also play significant roles in the optical behavior of AlN, but the contribution of Al vacancies remains uncertain, as they tend to form in high concentrations only in the presence of a substantial number of ionized donor impurities. Our investigation offers a new strategy and novel insights into the understanding of defect-induced optical properties in semiconductor materials.

II. METHODOLOGY

The simulations are carried out by applying our hybrid QM/MM embedded cluster method in the ChemShell package (Tcl version[47,48] and Python version[49]). The QM/MM system consists of five concentric regions/layers: (1) the innermost QM region; (2) a transition layer described by Gaussian-type pseudopotentials to compensate for force mismatches between the QM and MM regions and maintain a short-range embedding potential; (3) an "active" MM layer where all atoms and electron shells are relaxed; (4) a "frozen" MM layer, where atomic positions are fixed; and (5) an outermost layer of point charges added to reproduce the Madelung potential of the infinite crystal surrounding the defect center. DFT calculations are performed on an 86-atom cluster (~5 Å radius) using NWChem[50] for the QM region. Both the hybrid-level B97-2[51] and BB1K[52] exchange–correlation functionals are applied in this study as it has been previously reported that the fraction of the exact Hartree–Fock (HF) exchange significantly affects the

TABLE I. Overview of assignments of optical emission and absorption bands to native point defects in AlN found in the literature.

| Defect	Absorption/Emission	Energy (eV)	Refs.
V_{Al}	Absorption	2.1–2.9, 2.9–3.3	9
	Emission	2	10 and 11
		2.78, 3.4	9
		3.3	12–14
		4.6	15
V_N	Absorption	2.7–3.5	16
		3.4	17
		4.7	18
		5.0–5.8	19
	Emission	3, 3.2	20
		5	15
		5.87	21

energetics of defect formation and the positions of charge transition levels. Both have been fitted to large thermo-chemical datasets, with the B97-2 functional including 21% exact exchange, while the BB1K functional reproducing in addition selected reaction barriers includes 42% exact exchange and is expected to describe strongly localized states more accurately. The Def2-TZVP basis set[53] is used for both Al and N, with the outermost diffuse and high angular momentum basis functions removed to reduce computational cost. The MM simulations are performed using GULP.[54,55] The two MM regions contain ~10,000 atoms in total (~15 Å radius). Details on the technical aspects of our QM/MM method, such as the pseudopotential functions and the interatomic potential model used for other QM/MM regions, can be found in our previous studies.[46,56] In that previous work, the PBE0 functional,[57,58] which incorporates 25% exact exchange, was also employed. The resulting defect energies were found to lie at intermediate positions between those computed using B97-2 and BB1K, somewhat closer to those obtained with B97-2. We do not use the defect energies obtained from PBE0 in this study, instead focusing on those calculated using the B97-2 and BB1K functionals.

The Fermi levels are determined using a self-consistent method (code: SC-FERMI[59]) under the condition of overall charge neutrality, balancing the concentrations of free charge carriers and all defect species (charged and neutral). The equilibrium concentrations of all free charge carriers were calculated by integrating the electronic density of states (DOS) of AlN, obtained using VASP.[60–62] However, as the B97-2 and BB1K functionals are not available in plane-wave-based DFT codes at present, to our knowledge, the DOS of AlN was computed using the PBE0 functional. We obtained a bandgap energy of 6.11 eV using PBE0, close to the experimental gap value. Figure S1 in the supplementary material compares the Fermi levels calculated using defect concentrations from B97-2, PBE0, and BB1K functionals, all referenced against the PBE0-based DOS. The Fermi level obtained by PBE0 lies at a similar position to that from B97-2 and is lower than that from BB1K by less than 0.2 eV. For a wide-gap material of 6.11 eV, we consider that these are only minor differences between different functionals, so we use the Fermi level obtained from PBE0 in subsequent discussions.

III. RESULTS AND DISCUSSION

The charge transition levels obtained from the defect transition diagrams provide the energy levels of the single-electron transitions, considering only the predominant charged point defects while neglecting all other charge states and defect types. Figure 1 summarizes the charge transition levels (including all the meta-stable states) based on our defect transition diagram reported previously.[46] Matching our predicted charge transition levels to previous experimental assignments of optical signals remains challenging (see Table I: the reported V_{Al} signals at 2–4.6 eV and the V_N signals at 2.7–5.87 eV) due to the complexity of inequivalent defect sites and their charge states. Furthermore, when considering all the intrinsic defect types present in the material, our predicted self-consistent Fermi level is ~3.11–3.70 eV above the valence band maximum (VBM) under N-rich crystal growth conditions (4.67–5.19 eV for Al-rich conditions, shown in Fig. S1)[46] at 300–2800 K. The energy states below this value can be occupied, and electronic transitions can only occur between these states and the conduction band minimum (CBM) or shallow states near the CBM. For instance, considering a Fermi level of 3.66 eV under N-rich conditions at a growth temperature of 2800 K (a typical condition for bulk AlN crystal growth using physical vapor transport techniques[19,63,64]), multiple defect states remain between the VBM and the Fermi level (see Fig. 1), which still
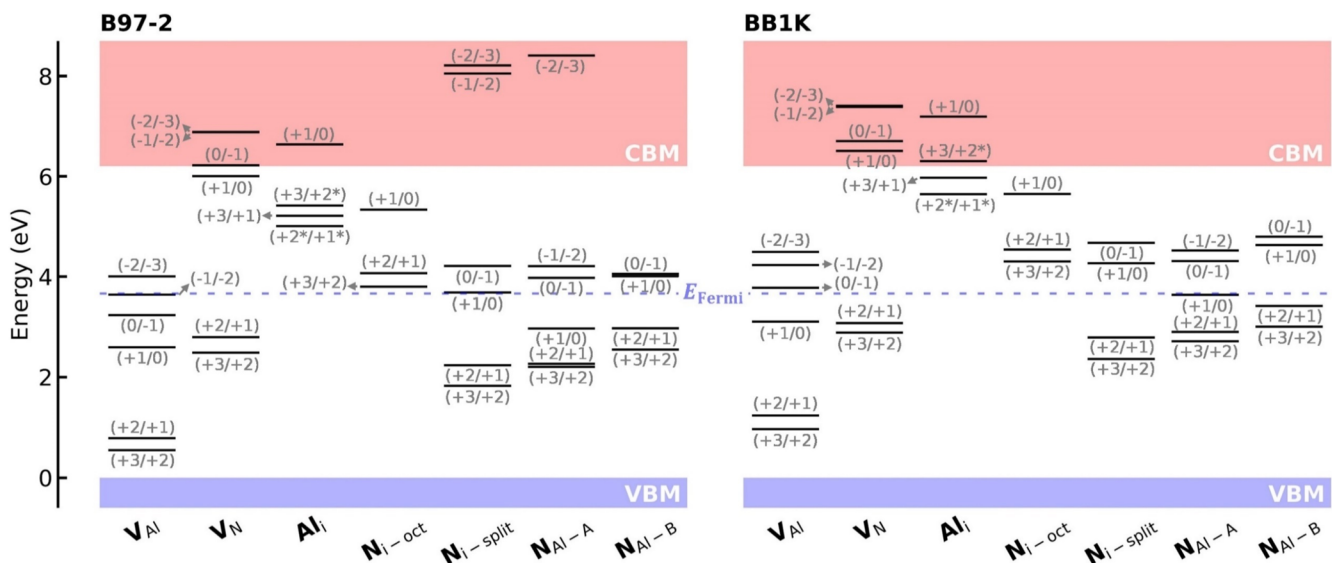
FIG. 1. The charge state transition levels of native point defects in AlN (see the corresponding defect transition diagram from our previous study[46]) calculated using B97-2 and BB1K DFT hybrid functionals for N-rich conditions. The charge states marked with asterisks (*) are the metastable states (which are structurally stable states from simulations but not the thermodynamically stable ones at any Fermi level within the bandgap). Note that the self-consistent Fermi level, E_{Fermi}, is calculated using the PBE0 functional at 2800 K (see more details in our previous study[46]).

makes it difficult to unambiguously assign specific defect species to experimentally observed optical signals.

Defects in different charge states undergo distinct lattice relaxations, whereas electronic transitions occur on much shorter timescales. Therefore, a clearer picture of electron and hole capture via charged defects is properly described by a configuration-coordinate diagram (Fig. 2), where free energy surfaces are plotted against the interpolated configurations between the equilibrium structures of two charge states. The process of optical absorption and its required energy (E_{AB}) is depicted as the excitation of an electron from the ground state to the excited state, while optical emission (and its photoluminescence (PL) energy, E_{PL}) corresponds to the capture of an electron from the excited state to the ground state. The energy difference between the minima of the two curves is the zero-phonon line (E_{ZPL}). As illustrated in Fig. 2, since opti-
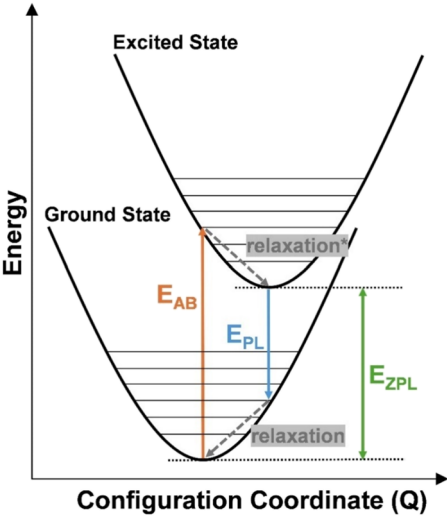
cal processes occur much faster than lattice relaxations, vertical lines between the two states represent these transitions, giving rise to the Stokes shifts between absorption and emission signals, which are commonly observed in experiments. The configuration-coordinate diagram is a common tool for identifying the defect origins of optical transitions in wide-gap materials.[65] It has previously been used to predict optical absorption/emission lines arising from Al vacancies, N vacancies, and O impurities in AlN.[34,40,44]

The optical transition energies between different charge states, i.e., E_{AB} and E_{PL}, are obtained by performing single-point QM/MM calculations by altering the net charge of the equilibrium structures. Here, we use $D(Q|Q + 1)e$ to denote an electron excitation transition (defect-to-CBM transition), where a defect species (D) changes from the ground state (charge Q) to the excited state (charge $Q + 1$) and $D(Q|Q - 1)h$ to represent a hole generating process (VBM-to-defect transition). All corresponding energies, including the equilibrium energies from structural relaxation (E_{rel} for relaxation in the ground state and E_{rel*} for the relaxation in the excited state), are summarized in Tables II–V.

We first discuss the optical properties of the nitrogen vacancy V_N^q, as it is the most stable defect type and a dominant donor species in AlN.[46,56] Using the B97-2 functional, we found a broad range of absorption energies (0.55–5.43 eV) associated with electron excitation from the V_N states to the CBM and from VBM to the defect states (Table II). When using BB1K optimized structures and energies, the defect states shift slightly closer to CBM, yielding absorption energies of 0.08–5.02 eV. In the literature, V_N was first assigned to an absorption band at 370 nm (~3.4 eV) as an F-centre defect.[17] Later, two absorption bands in the ranges of 5.0–5.8 eV and 2.7–3.5 eV were attributed to this defect,[16,19] and it was proposed that the defect is responsible for the yellow-to-red coloration of as-grown AlN crystal samples.[66] More recently, a study reported a 4.7 eV absorption signal by V_N.[18] From our calculations, while the bands at 3.4 eV and 2.7–3.5 eV do not correspond to any of our predicted transitions for V_N, the 5.0–5.8 eV band can be associated with the $V_N(+2|+3)e$ transition, and the 4.7 eV band is likely to be associated with the $V_N(+1|+2)e$ or the $V_N(+3|+2)h$ transition.

FIG. 2. A schematic representation of the configuration coordinate diagram.

TABLE II. Summary of ionization energies of nitrogen vacancy defect (V_N) for the full range of charge states using the B97-2 and BB1K functionals. The energy terms are defined in the main text, and all values are in eV.

Defect states	B97-2					BB1K				
	E_{PL}	E_{AB}	ZPL	E_{rel}	E_{rel*}	E_{PL}	E_{AB}	ZPL	E_{rel}	E_{rel*}
$V_N(+2|+3)e$	1.88	5.43	3.71	1.83	1.71	1.48	5.02	3.31	1.83	1.70
$V_N(+1|+2)e$	2.14	4.72	3.40	1.27	1.32	1.86	4.43	3.12	1.26	1.31
$V_N(0|+1)e$	−0.77	1.25	0.20	0.97	1.05	−1.25	0.73	−0.31	0.94	1.04
$V_N(-1|0)e$	−0.94	0.92	−0.02	0.92	0.94	−1.39	0.41	−0.50	0.89	0.92
$V_N(-2|-1)e$	−1.82	0.55	−0.68	1.14	1.23	−2.37	0.08	−1.21	1.16	1.29
$V_N(+3|+2)h$	0.77	4.32	2.49	1.72	1.83	1.19	4.72	2.89	1.70	1.83
$V_N(+2|+1)h$	1.48	4.07	2.80	1.32	1.27	1.77	4.34	3.08	1.31	1.26
$V_N(+1|0)h$	4.95	6.97	6.00	1.05	0.97	5.47	7.45	6.51	1.04	0.94
$V_N(0|-1)h$	5.28	7.14	6.22	0.94	0.92	5.79	7.59	6.70	0.92	0.89
$V_N(-1|-2)h$	5.65	8.02	6.88	1.23	1.14	6.12	8.57	7.41	1.29	1.16

TABLE III. Summary of ionization energies of aluminum vacancy defect (V_{Al}) for the full range of charge states using the B97-2 and BB1K functionals. The energy terms are defined in the main text, and all values are in eV.

Defect states	B97-2					BB1K				
	E_{PL}	E_{AB}	ZPL	E_{rel}	E_{rel*}	E_{PL}	E_{AB}	ZPL	E_{rel}	E_{rel*}
$V_{Al}(+2|+3)e$	3.95	6.95	5.65	1.70	1.30	3.15	6.92	5.24	2.09	1.68
$V_{Al}(+1|+2)e$	4.06	6.22	5.41	1.36	0.80	3.71	6.21	4.96	1.25	1.25
$V_{Al}(0|+1)e$	3.06	5.09	3.61	0.54	1.49	2.31	4.38	3.09	0.78	1.28
$V_{Al}(-1|0)e$	2.45	3.49	2.96	0.52	0.53	1.67	3.37	2.43	0.75	0.95
$V_{Al}(-2|-1)e$	1.67	3.43	2.56	0.89	0.87	0.86	3.14	1.97	1.11	1.17
$V_{Al}(-3|-2)e$	0.59	3.60	2.20	1.60	1.41	0.00	3.29	1.71	1.71	1.58
$V_{Al}(+3|+2)h$	−0.75	2.26	0.55	1.30	1.70	−0.72	3.05	0.97	1.68	2.09
$V_{Al}(+2|+1)h$	−0.02	2.14	0.79	0.80	1.36	−0.01	2.49	1.24	1.25	1.25
$V_{Al}(+1|0)h$	1.11	3.14	2.60	1.49	0.54	1.72	3.83	3.11	1.28	0.78
$V_{Al}(0|-1)h$	2.71	3.75	3.24	0.53	0.52	2.83	4.91	3.78	0.95	0.75
$V_{Al}(-1|-2)h$	2.77	4.53	3.64	0.87	0.89	3.06	5.34	4.23	1.17	1.11
$V_{Al}(-2|-3)h$	2.60	5.61	4.00	1.41	1.61	2.91	6.20	4.49	1.58	1.71

TABLE IV. Summary of ionization energies of aluminum interstitial defect (Al_i) for the full range of charge states using the B97-2 and BB1K functionals. The energy terms are defined in the main text, and all values are in eV.

Defect states	B97-2					BB1K				
	E_{PL}	E_{AB}	ZPL	E_{rel}	E_{rel*}	E_{PL}	E_{AB}	ZPL	E_{rel}	E_{rel*}
$Al_i(+2|+3)e$		3.12	0.78		2.33		2.44	−0.10		2.54
$Al_i(+1|+2)e$	−0.33	2.73	1.19	1.52	1.54	−1.13	2.22	0.56	1.68	1.66
$Al_i(0|+1)e$	−1.44	0.61	−0.44	1.00	1.05	−2.00	0.06	−0.99	1.01	1.05
$Al_i(+3|+2)h$	3.08		5.42	2.33		3.76		6.30	2.54	
$Al_i(+2|+1)h$	3.47	6.53	5.01	1.54	1.52	3.98	7.33	5.65	1.66	1.68
$Al_i(+1|0)h$	5.59	7.64	6.64	1.05	1.00	6.14	8.20	7.19	1.05	1.01

We identified two plausible emission processes in the infrared-to-visible spectrum from the CBM to V_N^q states: 1.88 and 2.14 eV using B97-2 and 1.48 and 1.86 eV from BB1K (Table II); as in several other cases, the excited states relax into stable configurations, resulting in free energy barriers to further electron capture, represented by negative PL energies. Additionally, we found a broad range of emission energies (0.77–6.12 eV) associated with electron recombination from the V_N states to the VBM. Two deep-ultraviolet (DUV) bands at 5 and 5.82 eV have been previously reported[15,21] and attributed to V_N. A more recent study[20] has assigned the 415 nm (~3.0 eV) and 390 nm (~3.2 eV) blue-to-UV luminescence to the F-center V_N. Comparing them to our results, the 5 and 5.82 eV bands can be associated with the $V_N(+1|0)h$, $V_N(0|-1)h$, and $V_N(-1|-2)h$ transitions, but we could not assign any of our emission energies to the 3 and 3.2 eV signals.

Aluminum vacancies (V_{Al}) are predicted to have the highest concentration in the presence of extra ionized donors in the material,[46] making them another probable source of defect-induced optical transitions. Sedhain *et al.* reported that $V_{Al}(-2|-3)h$ was responsible for the absorption at 2.1–2.9 eV and the emission at 2.78 eV.[9] Later, first-principles calculations using plane-wave-based basis functions and the HSE06 functional confirmed the value of this emission.[34] While our calculations predict no such absorption band associated with this transition, the reported emission band aligns well with our prediction at 2.60 and 2.91 eV using B97-2 and BB1K functionals for the $V_{Al}(-2|-3)h$ transition. Additionally, we found that $V_{Al}(-1|-2)h$ can also contribute to this emission signal (our prediction: 2.77 and 3.06 eV). However, we found that the absorption energies from the $V_{Al}(+3|+2)h$ and $V_{Al}(+2|+1)h$ transitions agree with the reported absorption bands. In the same study, $V_{Al}(-3|-2)e$ was assigned to the 2.9–3.3 eV absorption to the CBM,[9] which is close to our prediction range of 3.29 and 3.60 eV using B97-2 and BB1K. However, we also consider that the $V_{Al}(-2|-1)e$ transition, predicted at 3.14 and 3.43 eV, could contribute to this signal. Other optical transitions associated with V_{Al}-related signals have also been reported. The $V_{Al}(-1|-2)h$ transition was proposed as the origin of the 2 eV emission line.[11] However, our calculations predict a PL energy of 2.77 or 3.06 eV for this transition, ~0.7–1 eV higher than their observation. Nevertheless, the $V_{Al}(-1|-2)h$ and the $V_{Al}(0|+1)e$ transitions might be the source of the 3.3 eV emission signal reported by several studies.[12–14] The closest PL energy we predict is from the $V_{Al}(+1|0)h$ transition

22 September 2025 13:52:42

TABLE V. Summary of ionization energies of nitrogen split-interstitial defect ($N_{i-split}$) for the full range of charge states using the B97-2 and BB1K functionals. The energy terms are defined in the main text, and all values are in eV.

Defect states	B97-2					BB1K				
	E_{PL}	E_{AB}	ZPL	E_{rel}	E_{rel*}	E_{PL}	E_{AB}	ZPL	E_{rel}	E_{rel*}
$N_{i-split}(+2|+3)e$	1.88	6.23	4.37	2.49	1.85	1.24	6.03	3.84	2.60	2.19
$N_{i-split}(+1|+2)e$	2.01	5.37	3.96	1.96	1.40	1.30	5.17	3.41	2.11	1.76
$N_{i-split}(0|+1)e$	−1.58	3.92	2.52	4.10	1.41	−2.35	3.46	1.93	4.28	1.53
$N_{i-split}(−1|0)e$	0.69	2.80	1.99	1.30	0.82	0.14	2.31	1.53	1.39	0.78
$N_{i-split}(+3|+2)h$	−0.03	4.32	1.83	1.85	2.49	0.17	4.97	2.36	2.19	2.60
$N_{i-split}(+2|+1)h$	0.83	4.20	2.24	1.40	1.96	1.03	4.90	2.79	1.76	2.11
$N_{i-split}(+1|0)h$	2.28	7.79	3.69	1.41	4.10	2.74	8.55	4.27	1.53	4.28
$N_{i-split}(0|−1)h$	3.40	5.52	4.21	0.82	1.30	3.89	6.06	4.67	0.78	1.39

at 1.11 and 1.72 eV. However, since the concentration of positively charged V_{Al} is likely low in the material with high concentrations of ionized donors, the optical signal from this transition may be very weak.

One of the biggest challenges in assigning specific optical bands to V_{Al} in previous experimental studies is the presence of oxygen contamination in the samples. V_{Al} are often associated with oxygen substitutional defects (O_N), forming defect complexes. The higher the oxygen concentration, the more V_{Al} are likely to form in AlN. For instance, in the study of Sedhain et al.,[9] the oxygen concentration in the sample was measured to be ~2×10^{18} cm^{-3}, comparable to our calculated concentrations of intrinsic defects.[46] Our previous defect concentration calculations also indicate that V_{Al} becomes more prevalent than V_N only when additional ionized donors are present in the material,[46] which suggests that oxygen may play a crucial role in increasing the formation of V_{Al} in AlN. A more detailed QM/MM investigation into the effects of oxygen impurities will be explored in future studies.

We also calculated the optical transition energies for aluminum interstitial (Al_i) and nitrogen interstitial (N_i) defects, as these defects can reach high concentrations under specific chemical conditions, yet their optical properties remain largely unexplored. Most previous studies have overlooked interstitial-induced optical transitions, as early DFT studies using lower-level functionals suggested high formation energies for intrinsic interstitial defects. However, more recent simulations using hybrid-GGA-level functionals with spin polarization have shown that the formation energies of intrinsic interstitial point defects and interstitial-complex defects can be comparable to those of intrinsic vacancies.[46] From our previous calculations, positively charged Al_i was predicted to have a concentration comparable to V_N under N-rich conditions when high concentrations of ionized acceptors are precent.[46] For N_i, the nitrogen split-interstitial ($N_{i-split}$) configuration can form in concentrations comparable to V_N under N-rich conditions. (We will not expand on the other configuration, the octahedral-centric nitrogen interstitial, which is predicted to have high formation energies across all charge states, resulting in low concentrations.)[46]

Our calculations reveal several absorption bands associated with Al_i-to-CBM transitions, which are $Al_i(+2|+3)e$ (at 2.44 and 3.12 eV) and $Al_i(+1|+2)e$ (at 2.22 and 2.73 eV) (see Table III).

Notably, two previously reported experimental optical absorption signals at 2.7–3.5 eV and 2.1–2.9 eV, which were originally assigned to V_N and V_{Al}, respectively, can also be assigned to these transitions of Al_i. However, the emissions from both transitions are unlikely to be significant due to high free energy barriers (represented by the negative energies in Table IV). Additionally, we identified some possible defect-to-VBM emission bands at 3.08–3.98 eV, aligning with several experimentally observed bands previously attributed to V_{Al} (see the discussion above on V_{Al}). For $N_{i-split}$ (summarized in Table V), we found a wide range of visible-to-DUV absorption bands at 2.31–6.03 eV for defect-to-CBM transitions and DUV absorption bands at 4.20–8.55 eV for VBM-to-defect transitions. Predicted emission bands include 0.14–2.01 eV for CBM-to-defect transitions and 0.17–3.89 eV for defect-to-VBM transitions.

Based on the results presented above, we now provide a more global overview of defect-induced optical transitions in AlN. In an undoped system with only intrinsic point defects, the intrinsic Fermi level of AlN is predicted to lie between 3.11 and 3.70 eV under N-rich conditions and 4.67–5.19 eV under Al-rich conditions above the VBM.[46] This implies that defect states positioned between the VBM and the Fermi levels are fully occupied at low to moderate temperatures. As a result, only transitions either from occupied states below the Fermi level to the CBM or from the VBM to the unoccupied in-gap states above the Fermi level, with bands above 2.50 eV (N-rich) or above 1.01 eV (Al-rich) and below 6.11 eV (the bandgap value), can occur as one-particle processes. The most dominant defect species are V_N and $N_{i-split}$ under N-rich conditions and V_N under Al-rich conditions.[46] Under N-rich conditions, multiple transitions between the charge states of V_N and $N_{i-split}$ exhibit suitable absorption bands above 2.50 eV, as calculated using both B97-2 and BB1K functionals. Several emission transitions above 2.50 eV can also be assigned to V_N and $N_{i-split}$. Under Al-rich conditions, more transitions of V_N are identified, exhibiting both absorption and emission bands above 1.01 eV.

Next, we examine the conditions when a large number of ionized donors or acceptors are present in the material. When high concentrations of ionized donors are introduced, the Fermi level is predicted to shift to 5.00–5.76 eV under N-rich conditions and 6.12–6.41 eV under Al-rich conditions above the VBM.[46] In this case, the majority of in-gap states can contribute to optical

transitions, with possible transition bands appearing above 1.07 eV (N-rich) or above 0 eV (Al-rich) and below 6.11 eV. Under N-rich conditions, V_{Al} is the most dominant compensation defect.[46] Our calculations indicate that apart from $V_{Al}(+2|+3)e$ and $V_{Al}(+1|+2)e$ transitions, which are above 6.20 eV, all other absorption transitions of V_{Al} are allowed to occur. For emissions, excluding the $V_{Al}(-3|-2)e$, $V_{Al}(+3|+2)h$, and $V_{Al}(+2|+1)e$ transitions, all other transitions are allowed. Under Al-rich conditions, as the Fermi level shifts very close to the CBM, the 0–0.59 eV emission transition of $V_{Al}(-3|-2)e$ is now allowed.

When high concentrations of ionized acceptors are introduced, the Fermi level is predicted to shift to 1.74–2.36 eV under N-rich conditions and 3.14–4.62 eV under Al-rich conditions, relative to the VBM.[46] Consequently, optical transitions can occur with bands above 3.84 eV (N-rich) or above 1.58 eV (Al-rich) and below 6.11 eV. Under N-rich conditions, the predominant compensating defect is V_N, with increasing concentrations of Al_i and $N_{i\text{-split}}$ at elevated temperatures.[46] Multiple transitions between V_N charge states exhibit suitable absorption and emission bands, while additional transitions associated with $N_{i\text{-split}}$ also contribute to optical activity. No transition attributed to Al_i can be found in the energy range of 3.84–6.20 eV. Under Al-rich conditions, the concentrations of Al_i and $N_{i\text{-split}}$ decrease significantly, and V_N remains to be the most dominant compensating defect species.[46] Optical transitions are now primarily from V_N.

Finally, we revisit the optical bands that could not be initially assigned to our predictions. The 2, 3, 3.2, and 4.6 eV emission peaks have been previously observed in the AlN epitaxial layer[11,15] and in AlN nano-powder.[20] These signals may now be attributed to V_N, $N_{i\text{-split}}$, or V_{Al}, depending on the specific growth conditions. For the 2 eV emission observed in samples grown under N-rich conditions with low impurity concentrations,[11] several transitions predicted for the undoped scenario using the B97-2 functional are consistent with this observation (assuming a ±10% prediction uncertainty). These include CBM-to-defect transitions of $V_N(+2|+3)e$ at 1.88 eV, $V_N(+1|+2)e$ at 2.14 eV, $N_{i\text{-split}}(+2|+3)e$ at 1.88 eV, and

$N_{i\text{-split}}(+1|+2)e$ at 2.01 eV. Similarly, for the 4.6 eV signals also observed in N-rich grown epitaxial films,[15] the $V_N(+1|0)h$ transition at 4.95 eV (B97-2) is a likely contributing source. We note that our BB1K calculations for these transitions predict emission energies ~0.5 eV lower than the B97-2 functional. However, we may conclude that the source of the observed 2 eV peak is an N defect in AlN.

For the 3 and 3.2 eV emissions, which were observed in nanoparticle samples with significant levels of oxygen,[20] they may now be attributed to V_{Al} due to the increasing presence under conditions with high levels of ionized donors. A wide range of possible transitions involving V_{Al} are identified: $V_{Al}(+2|+3)e$ at 3.15 eV (BB1K), $V_{Al}(0|+1)e$ at 3.06 eV (B97-2), $V_{Al}(0|-1)h$ at 2.71 eV (B97-2) and 2.83 eV (BB1K), $V_{Al}(-1|-2)h$ at 2.77 eV (B97-2) and 3.06 eV (BB1K), and $V_{Al}(-2|-3)h$ at 2.91 eV (BB1K). These results suggest that V_{Al}, for most of its charge states, likely plays a substantial role in the blue-to-UV spectral range, which is critical for AlN-based blue-light and UV LED applications.

Finally, two absorption signals observed at 2.7–3.5 and 3.4 eV in single-crystal AlN, previously attributed to V_N, may now be reassigned based on our analysis. The former, observed in samples with high concentrations of oxygen, is more likely attributed to V_{Al}. The latter, observed in samples with high concentrations of carbon, may be assigned to $N_{i\text{-split}}(0|+1)e$ at 3.46 eV (BB1K) and $N_{i\text{-split}}(-1|0)e$ at 2.80 eV (B97-2) as no corresponding V_N transition matches within the energy range. These discrepancies, including the ones from our emission assignments, imply the dependence of predicted transition energies on the choice of DFT functionals. Consequently, the assignment of calculated transitions to experimentally observed optical signals is rather complex and uncertain. Therefore, we caveat these assignments with regard to the choice of functional, although note that the $N_{i\text{-split}}$ defect is predicted to be the source of these peaks, regardless of the functional in our study. Further refinement may be achieved by incorporating non-radiative recombination processes, which account for structural relaxations during electron and hole capture.

TABLE VI. Summary of our predicted assignments to experimentally observed optical signals in AlN. (Corresponding references are provided in Table I and discussed in the main text.)

	Energy (eV)	Predicted origin
Absorption	2.1–2.9	$V_{Al}(+2|+1)h$, $V_{Al}(+3|+2)h$
	2.9–3.3	$V_{Al}(-2|-1)e$, $V_{Al}(-3|-2)e$
	2.7–3.5	V_{Al} (charge transitions in the main text)
	3.4	$N_{i\text{-split}}(-1|0)e$, $N_{i\text{-split}}(0|+1)e$,
	4.7	$V_N(+1|+2)e$, $V_N(+3|+2)h$
	5.0–5.8	$V_N(+2|+3)e$
Emission	2	$V_N(+1|+2)e$, $V_N(+2|+3)e$, $N_{i\text{-split}}(+1|+2)e$, $N_{i\text{-split}}(+2|+3)e$
	2.78	$V_{Al}(-2|-3)h$, $V_{Al}(-1|-2)h$
	3, 3.2	V_{Al} (charge transitions in the main text)
	3.3	$V_{Al}(-1|-2)h$, $V_{Al}(0|+1)e$
	3.4	$V_{Al}(-2|-3)h$, $V_{Al}(-1|-2)h$
	4.6	$V_N(+1|0)h$
	5	$V_N(-1|-2)h$, $V_N(0|-1)h$, $V_N(+1|0)h$
	5.87	$V_N(-1|-2)h$, $V_N(0|-1)h$, $V_N(+1|0)h$

22 September 2025 13:52:42

IV. SUMMARY AND CONCLUSIONS

In summary, using the QM/MM embedded cluster method, we have investigated the optical properties of intrinsic vacancy and interstitial defects in AlN in an environment approaching the dilute limit. These advanced DFT methods provide more accurate formation energies of charged point defects and more precise energy levels of the defect states in the bandgap due to more precise treatment of long-range electrostatic interactions and ionization processes. By calculating the optical transition energies for vacancies and interstitials across the full range of charge states, we have reviewed all the previously observed optical bands and assigned them to our predicted transitions of defect species, which is summarized in Table VI. In contrast to previous studies, which considered only contributions from vacancy defects, our calculations suggest that interstitial defects can also play a significant role in the optical properties of AlN. Furthermore, depending on the chemical conditions of AlN crystal growth and the positions of the Fermi level, the dominant defect species and their contributions to optical properties can vary. We suggest that the nitrogen vacancies, which have the highest concentration under most of the chemical conditions, contribute most significantly to optical transitions in the material. For aluminum vacancies, while we found several optical signals could be associated with them, their contribution tends to emerge when a large number of ionized donors is present in the material. It is very likely that oxygen impurities enhance the presence of aluminum vacancies, resulting in stronger blue-to-UV optical transitions. Nitrogen split-interstitial defects play a secondary role, depending on their concentrations in the material. This study provides new insights into defect-induced optical transitions in both intrinsic and impurity-containing AlN, which can be beneficial for optoelectronic applications and quantum technologies.

SUPPLEMENTARY MATERIAL

The supplementary material provides an additional figure that supports the findings of this study. Figure S1 compares the self-consistent Fermi level predicted from the defect formation energies calculated by different DFT functionals (B97-2, PBE0, and BB1K).

AUTHOR DECLARATIONS

Conflict of Interest

The authors have no conflicts to disclose.

Author Contributions

Lei Zhu: Conceptualization (equal); Data curation (lead); Formal analysis (lead); Investigation (lead); Methodology (equal); Project administration (equal); Resources (equal); Supervision (equal); Validation (lead); Visualization (lead); Writing – original draft (lead); Writing – review & editing (lead). **Xingfan Zhang**: Investigation (equal); Methodology (equal); Validation (equal); Visualization (equal); Writing – review & editing (equal). **You Lu**: Methodology (equal); Software (equal); Writing – review & editing (equal). **Thomas W. Keal**: Methodology (equal); Software (equal); Writing – review & editing (equal). **John Buckeridge**: Conceptualization (equal); Formal analysis (equal); Investigation (equal); Methodology (equal); Software (equal); Writing – original draft (equal); Writing – review & editing (equal). **C. Richard A. Catlow**: Conceptualization (equal); Methodology (equal); Project administration (lead); Resources (equal); Software (equal); Supervision (lead); Writing – review & editing (equal). **Alexey A. Sokol**: Conceptualization (equal); Data curation (equal); Formal analysis (equal); Investigation (equal); Methodology (equal); Project administration (equal); Resources (equal); Software (equal); Supervision (equal); Writing – review & editing (equal).

DATA AVAILABILITY

The data that support the findings of this study are available within the article and its supplementary material.

REFERENCES

[1] W. Werdecker and F. Aldinger, "Aluminum nitride-an alternative ceramic substrate for high power applications in microcircuits," IEEE Trans. Compon., Hybrids, Manuf. Technol. **7**(4), 399–404 (1984).

[2] Y. Taniyasu, M. Kasu, and T. Makimoto, "An aluminium nitride light-emitting diode with a wavelength of 210 nanometres," Nature **441**(7091), 325–328 (2006).

[3] T. Takano, T. Mino, J. Sakai, N. Noguchi, K. Tsubaki, and H. Hirayama, "Deep-ultraviolet light-emitting diodes with external quantum efficiency higher than 20% at 275 nm achieved by improving light-extraction efficiency," Appl. Phys. Express **10**(3), 031002 (2017).

[4] M. Kneissl, T. Y. Seong, J. Han, and H. Amano, "The emergence and prospects of deep-ultraviolet light-emitting diode technologies," Nat. Photonics **13**(4), 233–244 (2019).

[5] M. Kneissl, Z. Yang, M. Teepe, C. Knollenberg, O. Schmidt, P. Kiesel, N. M. Johnson, S. Schujman, and L. J. Schowalter, "Ultraviolet semiconductor laser diodes on bulk AlN," J. Appl. Phys. **101**(12), 123103 (2007).

[6] T. Koppe, H. Hofsäss, and U. Vetter, "Overview of band-edge and defect related luminescence in aluminum nitride," J. Lumin. **178**, 267–281 (2016).

[7] Y. Xue, H. Wang, N. Xie, Q. Yang, F. Xu, B. Shen, J.-j. Shi, D. Jiang, X. Dou, T. Yu, and B.-q. Sun, "Single-photon emission from point defects in aluminum nitride films," J. Phys. Chem. Lett. **11**(7), 2689–2694 (2020).

[8] J. R. Weber, W. F. Koehl, J. B. Varley, A. Janotti, B. B. Buckley, C. G. Van de Walle, and D. D. Awschalom, "Quantum computing with defects," Proc. Natl. Acad. Sci. U. S. A. **107**(19), 8513–8518 (2010).

[9] A. Sedhain, L. Du, J. H. Edgar, J. Y. Lin, and H. X. Jiang, "The origin of 2.78 eV emission and yellow coloration in bulk AlN substrates," Appl. Phys. Lett. **95**(26), 262104 (2009).

[10]L. Shen, N. Wang, and X. Xiao, "Strong orange luminescence from AlN whiskers," Mater. Lett. **94**, 150–153 (2013).

[11]I. A. Aleksandrov, V. G. Mansurov, V. F. Plyusnin, and K. S. Zhuravlev, "Time-resolved photoluminescence characterization of 2 eV band in AlN," Physica Status Solidi C **12**(4–5), 353–356 (2015).

[12]R. A. Youngman and J. H. Harris, "Luminescence studies of oxygen-related defects in aluminum nitride," J. Am. Ceram. Soc. **73**(11), 3238–3246 (1990).

[13]T. Schulz, M. Albrecht, K. Irmscher, C. Hartmann, J. Wollweber, and R. Fornari, "Ultraviolet luminescence in AlN," Physica Status Solidi B **248**(6), 1513–1518 (2011).

[14]S. Tojo, R. Yamamoto, R. Tanaka, Q. T. Thieu, R. Togashi, T. Nagashima, T. Kinoshita, R. Dalmau, R. Schlesser, H. Murakami, R. Collazo, A. Koukitu, B. Monemar, Z. Sitar, and Y. Kumagai, "Influence of high-temperature processing on the surface properties of bulk AlN substrates," J. Cryst. Growth **446**, 33–38 (2016).

[15]B. Bastek, F. Bertram, J. Christen, T. Hempel, A. Dadgar, and A. Krost, "Analysis of point defects in AlN epilayers by cathodoluminescence spectroscopy," Appl. Phys. Lett. **95**(3), 032106 (2009).

[16]S. M. Evans, N. C. Giles, L. E. Halliburton, G. A. Slack, S. B. Schujman, and L. J. Schowalter, "Electron paramagnetic resonance of a donor in aluminum nitride crystals," Appl. Phys. Lett. **88**(6), 062112 (2006).

[17]K. Atobe, M. Honda, N. Fukuoka, M. Okada, and M. Nakagawa, "F-type centers in neutron-irradiated AlN," Jpn. J. Appl. Phys. **29**, 150–152 (1990).

[18]D. Alden, J. S. Harris, Z. Bryan, J. N. Baker, P. Reddy, S. Mita, G. Callsen, A. Hoffmann, D. L. Irving, R. Collazo, and Z. Sitar, "Point-defect nature of the ultraviolet absorption band in AlN," Phys. Rev. Appl. **9**(5), 054036 (2018).

[19]M. Bickermann, B. M. Epelbaum, and A. Winnacker, "Characterization of bulk AlN with low oxygen content," J. Cryst. Growth **269**(2–4), 432–442 (2004).

[20]B. Berzina, L. Trinkler, V. Korsaks, and R. Ruska, "Nitrogen vacancy type defect luminescence of AlN nanopowder," Opt. Mater. **108**, 110069 (2020).

[21]N. Nepal, K. B. Nam, M. L. Nakarmi, J. Y. Lin, H. X. Jiang, J. M. Zavada, and R. G. Wilson, "Optical properties of the nitrogen vacancy in AlN epilayers," Appl. Phys. Lett. **84**(7), 1090–1092 (2004).

[22]P. Boguslawski, E. Briggs, T. A. White, M. G. Wensell, and J. Bernholc, "Native defects in wurtzite GaN and AlN," MRS Proc. **339**(1), 693–698 (1994).

[23]T. Mattila and R. M. Nieminen, "*Ab initio* study of oxygen point defects in GaAs, GaN, and AlN," Phys. Rev. B **54**(23), 16676–16682 (1996).

[24]I. Gorczyca, A. Svane, and N. E. Christensen, "Calculated defect levels in GaN and AlN and their pressure coefficients," Solid State Commun. **101**(10), 747–752 (1997).

[25]I. Gorczyca, A. Svane, and N. E. Christensen, "Theory of point defects in GaN, AlN, and BN: Relaxation and pressure effects," Phys. Rev. B **60**(11), 8147–8157 (1999).

[26]A. Fara, F. Bernardini, and V. Fiorentini, "Theoretical evidence for the semi-insulating character of AlN," J. Appl. Phys. **85**(3), 2001–2003 (1999).

[27]C. Stampfl and C. G. Van de Walle, "Theoretical investigation of native defects, impurities, and complexes in aluminum nitride," Phys. Rev. B **65**(15), 155212 (2002).

[28]H. Seo, M. Govoni, and G. Galli, "Design of defect spins in piezoelectric aluminum nitride for solid-state hybrid quantum technologies," Sci. Rep. **6**(1), 20803 (2016).

[29]Y. Osetsky, M.-H. Du, G. Samolyuk, S. J. Zinkle, and E. Zarkadoula, "Native and radiation induced point defects in AlN and Sc-doped AlN," Phys. Rev. Mater. **6**(9), 094603 (2022).

[30]Y. Zhang, W. Liu, and H. Niu, "Native defect properties and *p*-type doping efficiency in group-IIA doped *wurtzite* AlN," Phys. Rev. B **77**(3), 035201 (2008).

[31]P. G. Moses, M. Miao, Q. Yan, and C. G. Van de Walle, "Hybrid functional investigations of band gaps and band alignments for AlN, GaN, InN, and InGaN," J. Chem. Phys. **134**(8), 084703 (2011).

[32]L. Silvestri, K. Dunn, S. Prawer, and F. Ladouceur, "Hybrid functional study of Si and O donors in wurtzite AlN," Appl. Phys. Lett. **99**(12), 122109 (2011).

[33]L. Gordon, J. L. Lyons, A. Janotti, and C. G. de Walle, "Hybrid functional calculations of DX centers in AlN and GaN," Phys. Rev. B **89**(8), 085204 (2014).

[34]Q. Yan, A. Janotti, M. Scheffler, and C. G. Van de Walle, "Origins of optical absorption and emission lines in AlN," Appl. Phys. Lett. **105**(11), 111104 (2014).

[35]A. Szállás, K. Szász, X. T. Trinh, N. T. Son, E. Janzén, and A. Gali, "Characterization of the nitrogen split interstitial defect in wurtzite aluminum nitride using density functional theory," J. Appl. Phys. **116**(11), 113702 (2014).

[36]J. B. Varley, A. Janotti, and C. G. Van de Walle, "Defects in AlN as candidates for solid-state qubits," Phys. Rev. B **93**(16), 161201 (2016).

[37]J. S. Harris, J. N. Baker, B. E. Gaddy, I. Bryan, Z. Bryan, K. J. Mirrielees, P. Reddy, R. Collazo, Z. Sitar, and D. L. Irving, "On compensation in Si-doped AlN," Appl. Phys. Lett. **112**(15), 152101 (2018).

[38]Y. Gao, D. Sun, X. Jiang, and J. Zhao, "Point defects in group III nitrides: A comparative first-principles study," J. Appl. Phys. **125**(21), 215705 (2019).

[39]K. Czelej, M. E. Turiansky, S. Mu, and C. G. Van de Walle, "Scandium-based point defect in AlN for quantum information processing," Phys. Rev. B **110**(12), 125116 (2024).

[40]Q. Yan, J. L. Lyons, L. Gordon, A. Janotti, and C. G. Van de Walle, "Oxygen impurities in AlN and their impact on optical absorption," Appl. Phys. Lett. **126**(6), 062106 (2025).

[41]S. Lany and A. Zunger, "Assessment of correction methods for the band-gap problem and for finite-size effects in supercell defect calculations: Case studies for ZnO and GaAs," Phys. Rev. B **78**(23), 235104 (2008).

[42]A. Walsh, "Correcting the corrections for charged defects in crystals," npj Comput. Mater. **7**(1), 72 (2021).

[43]J. M. Vail, D. Schindel, A. Yang, O. Penner, R. Pandey, H. Jiang, M. A. Blanco, A. Costales, Q. C. Qiu, and Y. Xu, "Effect of dielectric polarization on the properties of charged point defects in insulating crystals: The nitrogen vacancy in AlN," J. Phys.: Condens. Matter **16**(20), 3371 (2004).

[44]J. M. Vail, T. Haroon, J. Hernandez-Melgar, D. K. Chevrier, and R. Pandey, "Nitrogen vacancy and oxygen impurity in AlN: Spintronic quantum dots," Radiat. Eff. Defects Solids **164**(10), 585–591 (2009).

[45]A. A. Sokol, S. T. Bromley, S. A. French, C. R. A. Catlow, and P. Sherwood, "Hybrid QM/MM embedding approach for the treatment of localized surface states in ionic materials," Int. J. Quantum Chem. **99**(5), 695–712 (2004).

[46]L. Zhu, X. Zhang, Q. Hou, Y. Lu, T. W. Keal, J. Buckeridge, C. R. A. Catlow, and A. A. Sokol, "Formation of intrinsic point defects in AlN: A study of donor and acceptor characteristics using hybrid QM/MM techniques," J. Mater. Chem. A **12**(37), 25449–25464 (2024).

[47]P. Sherwood, A. H. de Vries, M. F. Guest, G. Schreckenbach, C. R. A. Catlow, S. A. French, A. A. Sokol, S. T. Bromley, W. Thiel, A. J. Turner, S. Billeter, F. Terstegen, S. Thiel, J. Kendrick, S. C. Rogers, J. Casci, M. Watson, F. King, E. Karlsen, M. Sjøvoll, A. Fahmi, A. Schäfer, and C. Lennartz, "QUASI: A general purpose implementation of the QM/MM approach and its application to problems in catalysis," J. Mol. Struct.: THEOCHEM **632**(1–3), 1–28 (2003).

[48]J. Kästner, J. M. Carr, T. W. Keal, W. Thiel, A. Wander, and P. Sherwood, "DL-FIND: An open-source geometry optimizer for atomistic simulations," J. Phys. Chem. A **113**(43), 11856–11865 (2009).

[49]Y. Lu, M. R. Farrow, P. Fayon, A. J. Logsdail, A. A. Sokol, C. R. A. Catlow, P. Sherwood, and T. W. Keal, "Open-source, Python-based redevelopment of the ChemShell multiscale QM/MM environment," J. Chem. Theory Comput. **15**(2), 1317–1328 (2019).

[50]E. Aprà, E. J. Bylaska, W. A. de Jong, N. Govind, K. Kowalski, T. P. Straatsma, M. Valiev, H. J. J. van Dam, Y. Alexeev, J. Anchell, V. Anisimov, F. W. Aquino, R. Atta-Fynn, J. Autschbach, N. P. Bauman, J. C. Becca, D. E. Bernholdt, K. Bhaskaran-Nair, S. Bogatko, P. Borowski, J. Boschen, J. Brabec, A. Bruner, E. Cauët, Y. Chen, G. N. Chuev, C. J. Cramer, J. Daily, M. J. O. Deegan, T. H. Dunning, K. G. Dyall, G. I. Fann, S. A. Fischer, A. Fonari, H. Früchtl, L. Gagliardi, J. Garza, N. Gawande, S. Ghosh, K. Glaesemann, A. W. Götz, J. Hammond, V. Helms, E. D. Hermes, K. Hirao, S. Hirata, M. Jacquelin, L. Jensen, B. G. Johnson, H. Jónsson, R. A. Kendall, M. Klemm, R. Kobayashi, V. Konkov, S. Krishnamoorthy, M. Krishnan, Z. Lin, R. D. Lins, R. J. Littlefield, A. J. Logsdail, K. Lopata, W. Ma, A. V. Marenich, J. Martin del Campo, D. Mejia-Rodriguez, J. E. Moore, J. M. Mullin, T. Nakajima, D. R. Nascimento, J. A. Nichols, P. J. Nichols, J. Nieplocha, A. Otero-de-la-Roza, B. Palmer, A. Panyala, T. Pirojsirikul, B. Peng, R. Peverati, J. Pittner, L. Pollack, R. M. Richard, P. Sadayappan, G. C. Schatz, W. A. Shelton, D. W. Silverstein, D. M. A. Smith, T. A. Soares, D. Song, M. Swart, H. L. Taylor, G. S. Thomas, V. Tipparaju, D. G. Truhlar, K. Tsemekhman, T. Van Voorhis, Á. Vázquez-Mayagoitia, P. Verma, O. Villa, A. Vishnu, K. D. Vogiatzis, D. Wang, J. H. Weare, M. J. Williamson, T. L. Windus, K. Woliński, A. T. Wong,

22 September 2025 13:52:42

Q. Wu, C. Yang, Q. Yu, M. Zacharias, Z. Zhang, Y. Zhao, and R. J. Harrison, "NWChem: Past, present, and future," J. Chem. Phys. **152**(18), 184102 (2020).

[51] P. J. Wilson, T. J. Bradley, and D. J. Tozer, "Hybrid exchange-correlation functional determined from thermochemical data and *ab initio* potentials," J. Chem. Phys. **115**(20), 9233–9242 (2001).

[52] Y. Zhao, B. J. Lynch, and D. G. Truhlar, "Development and assessment of a new hybrid density functional model for thermochemical kinetics," J. Phys. Chem. A **108**(14), 2715–2719 (2004).

[53] F. Weigend and R. Ahlrichs, "Balanced basis sets of split valence, triple zeta valence and quadruple zeta valence quality for H to Rn: Design and assessment of accuracy," Phys. Chem. Chem. Phys. **7**(18), 3297–3305 (2005).

[54] J. D. Gale and A. L. Rohl, "The general utility lattice program (GULP)," Mol. Simul. **29**(5), 291–341 (2003).

[55] J. D. Gale, "GULP: A computer program for the symmetry-adapted simulation of solids," J. Chem. Soc., Faraday Trans. **93**(4), 629–637 (1997).

[56] L. Zhu, C. R. A. Catlow, Q. Hou, X. Zhang, J. Buckeridge, and A. A. Sokol, "Computational study of native defects and defect migration in wurtzite AlN: An atomistic approach," J. Mater. Chem. A **11**(28), 15482–15498 (2023).

[57] J. P. Perdew, M. Ernzerhof, and K. Burke, "Rationale for mixing exact exchange with density functional approximations," J. Chem. Phys. **105**(22), 9982–9985 (1996).

[58] C. Adamo and V. Barone, "Toward reliable density functional methods without adjustable parameters: The PBE0 model," J. Chem. Phys. **110**(13), 6158–6170 (1999).

[59] J. Buckeridge, "Equilibrium point defect and charge carrier concentrations in a material determined through calculation of the self-consistent Fermi energy," Comput. Phys. Commun. **244**, 329–342 (2019).

[60] G. Kresse and J. Hafner, "*Ab initio* molecular dynamics for liquid metals," Phys. Rev. B **47**(1), 558–561 (1993).

[61] G. Kresse and J. Furthmüller, "Efficient iterative schemes for *ab initio* total-energy calculations using a plane-wave basis set," Phys. Rev. B **54**(16), 11169–11186 (1996).

[62] G. Kresse and D. Joubert, "From ultrasoft pseudopotentials to the projector augmented-wave method," Phys. Rev. B **59**(3), 1758–1775 (1999).

[63] G. A. Slack and T. F. McNelly, "Ain single crystals," J. Cryst. Growth **42**, 560–563 (1977).

[64] R. Yu, G. Liu, G. Wang, C. Chen, M. Xu, H. Zhou, T. Wang, J. Yu, G. Zhao, and L. Zhang, "Ultrawide-bandgap semiconductor AlN crystals: Growth and applications," J. Mater. Chem. C **9**(6), 1852–1873 (2021).

[65] R. Bai, Z. Lin, M. Huang, S. Wang, S. Chen, and Y.-N. Wu, "Identification of luminescent defects in wide-bandgap semiconductors using first-principles," J. Phys.: Condens. Matter **37**(29), 293001 (2025).

[66] V. A. Soltamov, I. V. Ilyin, A. A. Soltamova, D. O. Tolmachev, N. G. Romanov, A. S. Gurin, V. A. Khramtsov, E. N. Mokhov, Y. N. Makarov, G. V. Mamin, S. B. Orlinskii, and P. G. Baranov, "Shallow donors and deep-level color centers in bulk AlN crystals: EPR, ENDOR, ODMR and optical studies," Appl. Magn. Reson. **44**(10), 1139–1165 (2013).

22 September 2025 13:52:42